EVALUATION OF ANTIVASCULAR COMBRETASTATIN A4P EFFICACY BY USING SUPERSONIC SHEAR IMAGING TECHNIQUE OF ECTOPIC COLON CARCINOMA CT26

Johanne Seguin, Nathalie Mignet, Heldmuth Latorre Ossa, Mickaël Tanter, Jean-Luc Gennisson

EVALUATION OF ANTIVASCULAR COMBRETASTATIN A4P EFFICACY BY USING SUPERSONIC SHEAR IMAGING TECHNIQUE OF ECTOPIC COLON CARCINOMA CT26

Johanne Seguin[a], Nathalie Mignet[a], Heldmuth Latorre Ossa[b], Mickaël Tanter[b], and Jean-Luc Gennisson[b]*

[a] Paris Descartes University, Faculty of Pharmacy; Chimie ParisTech, Sorbonne Paris Cité; INSERM U1022, CNRS UMR8258; Chemical and Biological Technologies for Health Laboratory; 4 avenue de l'Observatoire, 75006 Paris, France

[b] Institut Langevin - Ondes et Images ; ESPCI Paris, PSL Research University, CNRS UMR7587, INSERM U979 ; 17, rue Moreau, 75012 Paris, France

*Corresponding author:
Jean-Luc Gennisson,
Institut Langevin – Ondes et Images
ESPCI Paris, PSL Research University, CNRS UMR7587, INSERM U979
17, rue Moreau,
75012 Paris, France
jl.gennisson@espci.fr
ph : +33 1 80 96 30 79

Abstract

A recent ultrasound imaging technique, called shear wave elastography, showed its ability to image and quantify mechanical properties of biological tissues, such as prostate or liver. In the present study this technique was used to evaluate the relation between tumor growth, stiffness and tumor reduction upon treatment with combretastatin (CA4P) in allografted colon tumor CT26, in mice. During twelve days, CT26 tumor growth (n=52) was imaged by ultrasound, and shear modulus was quantified, showing a good correlation between tumor volume and stiffness (r = 0.59). At day 12, the treatment was initiated and monitored every day during 4 days. Following the treatment, the tumor volume has decreased, still the elasticity parameter of the tumor volume was steady throughout the treatment. After segmentation using the shear modulus map, a detailed analysis showed a decrease in the stiffness after treatment as compared to the control group. This reduction in the mechanical properties was shown to correlate with tissue reorganization, in particular fibrosis and necrosis, assessed by histology.

Keywords: shear wave elastography, ultrafast ultrasound imaging, antivascular treatment, mice colon carcinoma model, histological parameters.

Introduction

Shear wave elastography (SWE) is an ultrasound imaging technique that allows imaging and quantification of the mechanical properties of soft tissues (Sarvazyan et al., 1998). Multiple variations of this technique have been developed throughout the years (Gennisson et al., 2013; Doyley et al., 2014) such as Shear wave Dispersion Ultrasonic Velocity (Chen et al., 2002), Acoustic Radiation Force Impulse (Nightingale et al., 2003) or Supersonic Shear Imaging (SSI) (Bercoff et al., 2004) which quantify or estimate the tissue stiffness. Stiffness of the human tissue is of great interest to physicians, since it relates to the palpation which is a basic step of the clinical exam. Few studies have shown that tumor stiffness quantification and mapping improves the physician diagnosis (Berg et al., 2012; Itoh et al., 2006; Lee et al., 2011). SWE was also applied in other organs such as the liver (Palmeri et al., 2008; Deffieux et al., 2015) and the prostate (Correas et al., 2013), showing the interest of quantifying the stiffness to better understand cancer pathologies.

Regarding cancer treatment, conventional ultrasound imaging is useful to quantify morphological tumor size evolution. However, it would be of great interest to add new imaging parameters that allow both early evaluation of the treatment and longitudinal monitoring. In this context, shear wave elastography can be a complementary technique providing informations on tissue viscoelastic properties, as an adjunct to conventional morphological ultrasound imaging. To our knowledge only a few studies have been done using shear wave elastography to follow cancer treatment. In 2013 and 2015, Evans and Athanasiou, respectively, used the SSI technique to follow breast cancer chemotherapy in humans (Evans et al., 2013; Athanasiou et al., 2015). These studies concluded that tumor stiffness can be a striking factor to predict chemotherapy treatment efficiency, since tumor stiffness was shown to decrease faster during treatment than the tumor volume assessed by conventional ultrasound.

Notwithstanding, it still remains challenging to understand the relationship between the macroscopic changes and the tissue remodeling due to the treatment. Regarding histological parameters, recent studies involving SWE results and breast tumor histological analysis have found controverting results. Chang et al. found that mucinous cancer in humans, which is often classified as softer lesions by pathologists, showed higher stiffness values than other types of breast cancer (Chang et al., 2011). Evans et al. demonstrated a relationship between SWE findings and histological prognostic factors (Evans et al., 2012). However, this study was not explicit on the tumor pathological features underlying the stiffness phenomenon. In order to better understand these issues, few studies have been conducted to characterize breast cancer at different stages. In a preclinical study, Chamming's et al. linked the changes in SWE to an increased fibrosis during tumor growth (Chamming's et al., 2013). Moreover, some authors showed a correlation between the SWE values and immune-histochemical profiles of invasive human breast cancer (Youk et al., 2013; Ganau et al., 2014). However, treatment monitoring has not been performed by using SWE methods. Likewise, clinical results of SWE reported in humans (Athanasiou et al., 2015), were not correlated to any histological parameters (Chamming's et al., 2015).

The aim of this study is to investigate the link between histopathological characterization and SWE measurements by using SSI techniques during antivascular treatment in a murine colon carcinoma model (CT26). This model was selected based on recent histo-pathological studies, which showed both well vascularized tumor and cellular adhesion molecules (CAM). CAMs are important targets for anti-angiogenic therapies, involved in the process of angiogenesis for tumor growth, cell migration and metastasis (Seguin et al., 2012). Combretastatin A4 phosphate (CA4P) was chosen as it is a particular effective antivascular drug, with an early post treatment effect (El-Emir et al., 2005). This vascular disrupting agent CA4P was described to induce a necrosis at the center of the tumor and a fibrosis at the viable

rim in periphery of the tumor (Dark et al., 1997), where necrosis is defined by a passive, accidental cell death resulting from environmental perturbations (Fink et al., 2005) and fibrosis by an overgrowth, hardening and/or scarring of various tissues attributed to an excessive deposition of extracellular matrix components including collagen (Wynn et al., 2008).

In the present study, the efficacy of antivascular treatment and the global stiffness were evaluated with conventional US and SSI technique respectively. Histological analyses were conducted at each stage to link the SWE results to changes in vascular density, cellularity and/or fibrosis.

Materials and Methods

Animal model

Fifty two 8-week-old female Balb-C mice with a mean weight of 20 g (Janvier, Saint Genest de l'Isle, France) were implanted with CT26 tumor fragment (3 mm^3) subcutaneously into the flank (n = 52) as previously described (Seguin et al., 2013). After implantation, the growth of the tumor was imaged with ultrasound from day 5 to day 12. All animals received animal care in compliance with the European Communities Council Directive of 2010. This study was approved by the local committee for animal care (Comité d'éthique en matière d'expérimentation animale n°34, Saisine 12-175, 'Paris Descartes') and received the agreement number # CEEA34.JS.142.1. In the experimental protocol certain parameters were established such as, weight loss higher than 20%, hostility between animals, abnormal behavior, shaggy fur, etc... In these cases the animals were sacrificed and excluded from the study.

Combretastatin A4 treatment

At day 12, 13 and 14 after tumor implantation half of the mice (n=26) were injected intraperitoneally with 100 mg/kg of CA4P disodium salt (Toroma Organics, Saarbrücken,

Germany) dissolved in sterile saline solution (10µl/g). The other 26 mice were used as a control group and received 10µl/g of saline solution.

Ultrasound (US) imaging

Ultrasound imaging was performed on each day of the treatment using an ultrafast ultrasound device (Aixplorer, Supersonic Imagine, Aix en Provence, France) with a framerate of 20000 images/s. The images were acquired using a high-frequency ultrasound probe (central frequency 15 MHz, 256 elements, 125 µm pitch, Vermon, Tours, France). Before performing the acquisitions, the mice were anesthetized using a gas mixture of isoflurane at 1.5% isoflurane (Aerrane®; Baxter S.A.S, France), oxygen (0.5 l/min) and air (1 l/min) and were subsequently shaved. Body temperature was monitored and controlled during the length of acquisition.

By using classical ultrasound imaging, B-mode, the operator localized the tumor within the imaging plane in real time by placing the probe on the anaesthetized mice. Once the probe was set up, ultrasound B-mode imaging was performed in order to define tumor morphology. This acquisition involved 2 perpendicular B-mode imaging planes (transverse and sagittal). The probe was oriented until the tumor size was maximized, for each acquisition at different time points (Seguin et al., 2013).

Thus, three diameters (two in the axial and one in the sagittal planes) were recorded, giving access to volume quantification according to the following ellipsoid formula $(\pi/6)\times L\times W\times H$, where H is the height , L is the length and W is the width in centimeters. (Cheung et al., 2005).

The SSI technique was used to measure the mean tumor stiffness under the assumption that the tissue is isotropic, locally homogeneous and purely elastic (Bercoff et al., 2004). Stiffness values were directly reported by the commercial system. Elastography images were then acquired daily during the treatment of the animals with the Combretastatin A4 P agent in

the central-sagittal and central-transversal planes of the tumors. In order to adjust the stiffness contrast on the image, the colorbar of the Aixplorer device was fixed between 0 and 40 kPa, with the pixels in blue and red representing the lowest and highest elasticity values, respectively. The clinical interface of the Aixplorer provides a Young's modulus value under a soft tissue hypothesis. Nevertheless in this paper we present the results of the Shear Modulus which is 1/3 of the Young's Modulus, between 0 and 13.3 kPa (Sarvazyan et al., 1998). The regions of interest (ROIs) were placed so as to cover the maximum surface of the tumor within the imaging plane. These ROIs (called Qbox™ in the Aixplorer device) were circular as defined in the clinical interface. An average of 2-3 region of interest (ROI) measurements in 6 images, taken on 2 different planes, was calculated to obtain the value of the global elasticity for each animal on each day. In the aim of refining analysis, B-mode images were then manually segmented by using a homemade software developed in Matlab (Mathworks, 2014a, Natick, Massachussets, USA). The resulting segmentation was used on the stiffness image to calculate mean values of stiffness and standard deviation in each segmented region. Thus global measurements obtain with the ROIs (Qbox™) are different from the global ones obtained with segmentation as they do not represent the same surface.

Histological analysis

The impact of CA4P treatment 12 days after tumor graft was evaluated by histology. At each time point of kinetics (day 13, 14 and 15) 3 mice of each group (control and treated) were sacrificed, tumor was removed and quickly frozen in liquid nitrogen. Ten-micron frozen tissue sections were placed on Polysine slides (Polysine®, CML, Nemours, France) and conserved in -80°C before analysis. For each tumor, histological analysis was obtained in the central slice of the tumor. In this slice, ten representative images were undertaken and analyzed. All stains were

performed at the same time and image digitization was made under identical lighting conditions to insure that analyses from different slides were comparable.

Microvascular density (MVD) immunostaining for the evaluation of the vascularization was performed using a CD31 (PECAM1) labeling consisting in a three-step procedure as previously described (Youk et al., 2013; Seguin et al., 2013; Nico et al., 2008). The quantification of the tumor vascularization was done using ImageJ software (version 1.50h) (Abramoff 2004). The result was expressed in number of vessels per square millimeter (mm^2). This parameter was referred to as MVD (microvascular density) in this paper. In order to improve the quantification, a specific macro under ImageJ software was built to segment images (appendix).

For necrosis assessment the haematoxylin eosin counterstain was performed (Robl et al., 2016). The slides were washed in distilled water and fixed 20 min with paraformaldehyde 4% in phosphate buffer. The slides were then cleaned out with running tap water for 5 minutes and stained in haematoxylin solution for 1 minute. A differentiation was made in saturated solution of lithium for 5 minutes. Then, the slides were stained with eosin for 30 seconds. Finally, they were dehydrated in alcohol and mounted with Eukitt® (Eukitt® quick-hardening mounting medium, Sigma-Aldrich Chemie S.a.r.l, Saint-Louis, Missouri, USA). Two different analyses of the necrosis were performed, global assessment of necrosis and percentage of necrosis in the local areas (center and edges). Firstly, global assessment of necrosis was calculated from dividing the necrosis area (pink zone in the image (fig. 4A, 4B)) by the total surface of the tumor. The necrosis area was obtained by drawing manually the eosin staining zones on images acquired at x25 magnification. Secondly, in order to get a value of necrosis in the edge and in the center of the tumor, a quantification of the number of pink staining area per square millimeter (mm^2) were done in 5 hot spots. These 5 hot spots were images at x200 magnification selected in 5 discrete locations within one slide per animal (appendix 2).

For fibrosis assessment: collagen fibers were stained with a Masson's trichromic coloration staining kit (Masson's Trichrome Stain Kit 25088-1, Polysciences Europe GmbH, Eppelheim, Germany) with some modifications adapted to immune-histochemical frozen samples as described below. The slides were washed in distilled water and fixed during one hour with paraformaldehyde 4% in a phosphate buffer. These slides were re-fixed in Bouin's solution for 5 min at 56°C followed by a supplementary incubating of 15 min at room temperature in order to improve the staining quality. The slides were washed with running tap water for 5 minutes to remove the yellow color, and stained with Weigert's iron haematoxylin working solution for 10 minutes and with Biebrich scarlet-acid fuchsin solution for 5 minutes. The differentiation was made in phosphomolybdic-phosphotungstic acid solution for 10 minutes. The slides were then directly stained with aniline blue solution for 5 minutes, cleaned out briefly in distilled water and differentiated in 1% acetic acid solution for 2-5 minutes. In order to obtain the value of the fibrosis in the edges and the center of the tumor, a quantification of the aniline blue staining was performed in 5 hot spot pictures in the center or in the edges of the tumor.

Statistical analysis

Statistical Two-way ANOVA with Bonferroni post-tests were performed with Graphpad software (Prism 5.01) to compare the control group and the treated group. Two-way ANOVA determines how a response is affected by two factors: drug treatment and time. Bonferroni post-tests were used to compare the control and the treated value at each time point. P values lower than 0.05 ($P < 0.05$) were considered as statistically significantly different.

In the interest of compared different parameters in each condition, Spearman's rank correlation has been applied, which makes no assumption about the distribution of the value, but is based on ranks of the value.

At last the evolution of the relative difference in stiffness (RD_{stiff}) regarding the first day of treatment was calculated by using the following formula:

$$RD_{stiff} = \frac{(Eday_x - Eday_{12})}{Eday_{12}}, \quad \text{Eq. (1)}$$

where $Eday_x$ is the mean shear modulus in kPa at day *x*. This approach allowed us to quantify the evolution of stiffness on the global population independently for each mouse.

Results

Shear wave elastography

On figure 1 is presented a shear modulus map (Fig. 1A) and a classical ultrasound image (Fig. 1B) for one mouse. A ROI is placed on the shear modulus map covering the maximum surface of the tumor. The mean stiffness value, maximum stiffness value, minimum stiffness value and standard deviation values were extracted from each ROI (respectively on figure 1A: 5.1 kPa, 11.7 kPa, 1.0 kPa, 2.3 kPa). These values are averaged over multiple acquisition images as described above providing the shear modulus mean values for each animal and day (presented in figure 2B).

Characterization of CT26 tumor stiffness as a function of time

As shown in figure 2A, the tumor volume increased over time as previously observed (Seguin et al., 2013). The shear modulus obtained by ultrasound imaging measurements also increased with the tumor growth (Figure 2B).

A positive correlation ($r=0.59$, $p<0.0001$) was obtained between tumor volume and the shear modulus parameter.

Effect of Combretastatin A4P treatment

Following the correlation between growth and stiffness, the effect of combretastatin on tumor growth and elasticity changes was evaluated by shear wave elastography. Measurements of tumor volume and elasticity post-combretastatin treatment were performed (Figure 3A and 3B). After CA4P treatment tumor volume did not increase from day 13 to day 15, while a significant growth was noticed in the untreated control group. No change was measured in terms of stiffness for both the treated and untreated groups. These results showed no correlation between stiffness and volume for both groups ($r < 0.01$ control, $r = 0.05$ CA4P), in opposite to what was observed prior day 12.

On figure 4A and 4B are presented histological slices of representative control tumor and treated tumor respectively. An increase of the global necrotic area in the tumor between control group and CA4P group was detected (Figure 4C, for example from 20.8±3.3 % to 52.6±3.0 % at day 13). On figures 4D and 4E are presented microscopic histological analyses (200x), of the CD31 labeling in control and treated tumors respectively. The effect on vascular density was found to be statistically different between the second and the third day of the treatment (Figure 4F), in accordance to what was previously found (Tozer et al., 1999).

Data refinement

Histological analysis of data revealed significant changes, thus a refinement of the stiffness analysis using normalization and segmentation of stiffness maps was made. After normalization of the relative difference of stiffness as a function of the first day of treatment (day 12) for each mouse, it is possible to observe a difference in the stiffness evolution between both groups (Table 1). The stiffness values in the control group remained higher than the treated group.

The value of shear modulus was obtained for the complete tumor area, and the effect of the combretastatin is known to preferentially impact the center and leave a viable rim in

periphery of the tumor. Therefore, refinement of the analysis and evaluation of various segmentations of the SWE images was applied. Figure 5 shows the stiffness map (A) and the ultrasound B mode image (B) for a tissue sample were the segmentation of the edges and the center was depicted on C (blue drawing) for one tumor.

The stiffness values were compared between global, center and edges of the tumor as a function of time (Fig. 5 D, E, F). Regarding the global stiffness of the control mice, stiffness changes significantly only after 15 days post implantation and 3 doses of combretastatin A4P. This difference is clearer by looking specifically at the edges values (Fig. 5E) after map segmentation.

Histological data for fibrosis and necrosis measurements are presented in Tables 2 and 3, respectively. Results were obtained on 5 random images in the center the tumor and on 5 random images in the edges of the tumor. These images were acquired in the histological slices in order to correspond to the imaging plane. On Table 2, it can be appreciated that the percentage of necrosis in the treated group increased as compared to the control group particularly in the center of the tumor. On the other hand Table 3 shows that the fibrosis score is negligible in the center and smaller than 2.5% on the edges in the control group. Meanwhile fibrosis increases as a function of time in the treated group within the whole tumor and more drastically in the edges of the tumor.

Discussion

In this study, CT26 tumors were analyzed using SWE and histological techniques in order to assess stiffness, fibrosis, necrosis and vascularization, as a function of time.

Regarding stiffness, values were taken directly from the Aixplorer device which assumes that medium are isotropic and purely elastic. However potential guided shear wave can propagate in small layers, but this was not investigated. In fact guided shear wave can lead

to a lower estimate of the shear wave speed (Nguyen et al., 2011; Brum et al., 2014) but this assumption was not taken into account in the present study.

As previously reported in the literature, stiffness increases with growing tumors (Seguin et al., 2013). This was also observed in allografted breast cancer tumors (HBCx-3) by Chamming's et al. (2013). A good correlation (r= 0.59) was found between volume assessment and stiffness with a Spearman's rank correlation analysis. This result is consistent with the study from Viana et al. who found that histological sections of CT26 tumor showed dense mass of tumor cells with poor fibrovascular tissue (Viana et al., 2013).

Regarding only stiffness evolution as a function of time, multiple studies were performed to better understand tumor behavior with treatment. In a clinical study, Athanasiou et al. showed that stiffness assessment could help to monitor chemotherapy (Athanasiou et al., 2015). However, this study was performed in a limited number of patients (n=10). In a preclinical study by Juge et al, they observed using Magnetic Resonance Imaging, that the tumor stroma in CT26 tumor represent only 10% of tumor area (Juge et al., 2012). In the same work it was shown that the percent of proliferative cells increased from day 5 (28.88 ± 2.35%) to day 11 (39.59 ± 3.92%). The cellularity increased significantly between day 5 (4775 ± 127 mm^2) and day 11 (5917 ± 398 mm^2; P = .03). The microvascular density also increased significantly from day 5 (224 ± 3 mm^2) to day 11 (299 ± 37 mm^2, P < .01). Therefore, the increased stiffness obtained by SWE from day 5 to day 12 in the present study is consistent with the modification of cellular and microvascular density previously reported in the literature. The aim of this study was to better understand histological and stiffness changes over a longer treatment period consisting of repeated administration of the antivascular drug (CA4P).

In figures 4A, 4B, a significant necrotic area was found in the center of the treated tumors (pink histological sample) following three days repeated injection of CA4P. This was also reported in the literature (Ganau et al., 2014; Juge et al., 2012). The corresponding data

quantification presented in figure 4C was about 50 % and 20 % for treated and control tumors respectively. Moreover, regarding MVD, the control group slightly increase as a function of time while the treated group remained constant (fig. 4F). This was consistent with a lack of vascularization resulting in some hypoxic areas which in turn led to necrosis. The level of necrosis impacts the correlation between the tumor volume and the shear modulus for both the control group and the treated group (Fig. 3A). Therefore, a poor correlation between stiffness and volume was found for both groups (r=0.00 control, r = 0.05 CA4P) between days 13 and 15.

Changes in stiffness and relation with histological results are not so straightforward to explain as tumor heterogeneity, in particular necrosis, plays a major role (Viana et al., 2013). Using manual segmentation of the stiffness maps (Figure 5C), instead of a circular ROI available on the Aixplorer device at the time of the study, allowed refining more precisely the data leading to significant differences between control and treated groups at day 15. By using this refinement, the stiffness values did not vary significantly in the center for both groups but changed significantly in the edges. Interestingly, a significant difference in stiffness was found between the control group and the treated group at days 14 and 15. This is consistent with the well-known formation of a viable rim described after CA4P treatment (Tozer et al., 1999). To go into further details, histological parameters and stiffness was simultaneously investigated. Changes in stiffness were reflected by histological data (Tables 2&3). A strong necrosis both in the center and in the edges was observed only for the treated group. A variation in fibrosis was also evidenced for the treated group, although, this discrepancy was less important than necrosis. Therefore for repeated administration of CA4P necrosis was the main factor explaining the stiffness differences.

Conclusion

In this study, stiffness was found to be slightly lower after CA4P treatment and could be related to modification in tissue organization like necrosis and fibrosis. The stiffness could directly highlight changes in the growing tumor between days 5 and 12 corresponding to more homogeneous tissue. After day 13, tumors are more heterogeneous due to the formation of various areas (hypoxic zone, fibrosis, and necrosis) which require refining the analysis of the SWE images to be able to detect stiffness discrepancies.

Acknowledgment

This work was supported by LABEX WIFI (Laboratory of Excellence ANR-10-LABX-24) within the French Program “Investments for the Future” under reference ANR-10-IDEX-0001-02 PSL, INSERM and CNRS funding. The authors thank R. Lai-Kuen, B. Saubamea and V. Mignon from the Technical Platform Cellular & Molecular Imaging and I. Dubai from the Animal Platform, CRP2 - UMS 3612 CNRS - US25 Inserm-IRD – Faculté de Pharmacie de Paris, Université Paris Descartes, Paris, France.

The authors would like to thank Dr. Miguel Bernal for useful discussions.

Appendix 1

The ImageJ script used was a homemade macro dedicated to segment histological parameter mainly based on contrast and color. The script was the following:

```
run("Enhance Contrast", "saturated=4 equalize"); run("Subtract Background...", "rolling=100 light"); run("Despeckle"); run("Color Threshold..."); title = "binarization of vessels"; msg = "If necessary, use the \"Threshold\" tool to\adjust the threshold, then click \"OK\"."; waitForUser(title, msg); run("8-bit"); setMinAndMax(69, 255); run("Make Binary"); run("Outline"); run("Analyze Particles...", "size=20-30000 circularity=0.00-1.00 show=Outlines summarize");
```

Threshold Color parameter:

Hue 41-233 pass untick, Saturation 84-255 pass tick, Brightness (automatic) pass tick, Thresholding method : Default, Threshold color B&W, Color space HSB

Appendix 2

Histological method used for necrosis assessment:

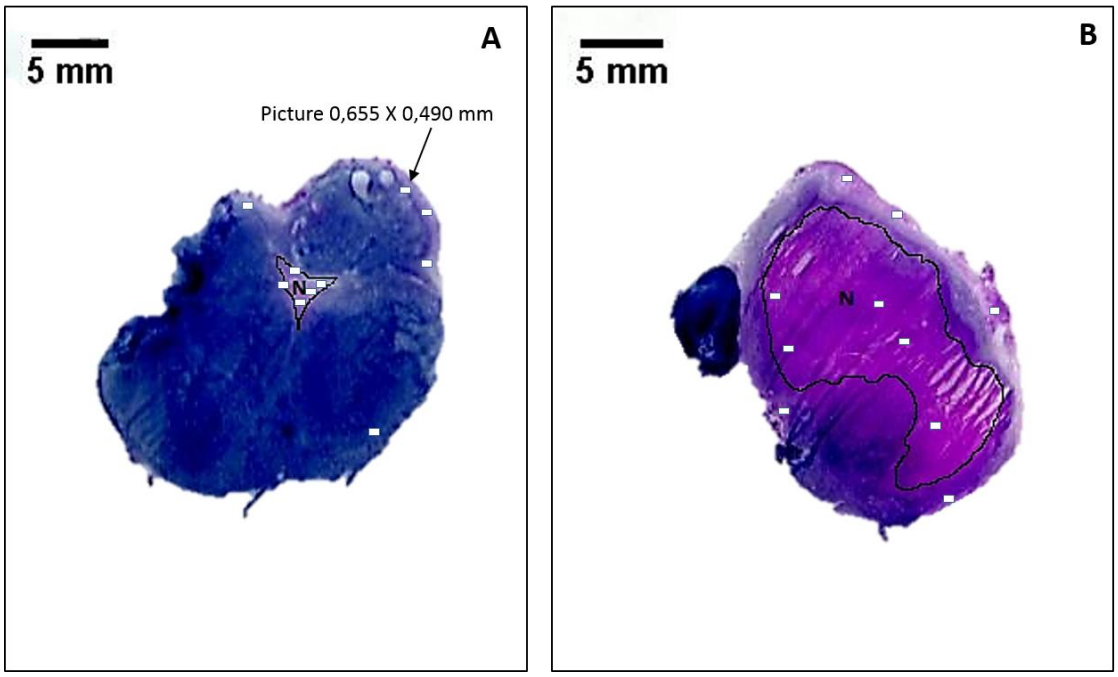

Percentage of global necrosis: this percentage was calculated from dividing the necrosis area (pink zone in the image (noted N)) by the total surface of the tumor. The necrosis area was obtained by drawing manually the eosin staining zones on images acquired at x25 magnification.

Percentage of necrosis in the local areas: an evaluation of necrosis in the center and in the edges was made in 5 hot spots. These 5 hot spots, were placed in the pink area located on the edge and the center. An example of the positioning of theses hot spots was represented here (white square), images was made at x200 magnification and have consequently a size of 0.655 x 0.490 mm.

Conflict of interest statement

M.T. is cofounder and shareholder of Supersonic Imagine Company. J.L.G. is scientific consultant for Supersonic Imagine.

References

Abràmoff M. Image processing with ImageJ. Biophotonics Int 2004; 11:36–42.

Athanasiou A, Latorre-Ossa H, Criton A, Tardivon A, Gennisson JL, Tanter M. Feasibility of Imaging and Treatment Monitoring of Breast Lesions with Three-Dimensional Shear Wave Elastography.". Ultraschall Der Medizin, 2015; DOI: 10.1055/s-0034-1398980.

Bercoff J, Tanter M, Fink M. Supersonic shear imaging: A new technique for soft tissues elasticity mapping. IEEE Trans Ultrason Ferroelectr Freq Control 2004;51(4):396–409.

Berg WA, Cosgrove DO, Doré CJ, Schäfer FKW, Svensson WE, Hooley RJ, Ohlinger R, Mendelson EB, Balu-Maestro C, Locatelli M, Tourasse C, Cavanaugh BC, Juhan V, Stavros AT, Tardivon A, Gay J, Henry JP, Cohen-Bacrie C, BE1 Investigators. Shear-wave elastography improves the specificity of breast US: the BE1 multinational study of 939 masses. Radiology 2012;262:435–449.

Brum J, Bernal M, Gennisson JL, Tanter M. In vivo evaluation of the elastic anisotropy of the human Achilles tendon using shear wave dispersion analysis. Phys. Med. Bio. 2014;59(3):505-523.

Chamming's F, Latorre-Ossa H, Le Frère-Belda M, Fitoussi V, Quibel T, Assayag F, Marangoni E, Autret G, Balvay D, Pidial L, Gennisson JL, Tanter M, Cuénod CA, Clément O, Fournier LS. Shear wave elastography of tumour growth in a human breast cancer model with pathological correlation. Eur Radiol 2013;23:2079–86.

Chamming's F, Le-Frère-Belda M-A, Latorre-Ossa H, Fitoussi V, Redheuil A, Assayag F, Pidial L, Gennisson JL, Tanter M, Cuénod CA, Fournier LS. Supersonic Shear Wave Elastography of Response to Anti-cancer Therapy in a Xenograft Tumor Model. Ultrasound Med Biol 2015;42:924–30.

Chang JM, Moon WK, Cho N, Yi A, Koo HR, Han W, Noh DY, Moon HG, Kim SJ. Clinical application of shear wave elastography (SWE) in the diagnosis of benign and malignant breast diseases. Breast Cancer Res Treat 2011;129:89–97.

Chen S, Fatemi M, Greenleaf J. Shear property characterization of viscoelastic media using vibrations induced by ultrasound radiation force. Proc IEEE Int Ultrason Symp 2002;2:1871–5.

Cheung MY, Brown S, Hastie L, Cucevic V, Roy M, Lacefield JC, Fenster A, Foster FS. Three-dimensional ultrasound biomicroscopy for xenograft growth analysis. Ultrasound Med Biol 2005;31:865–70.

Correas JM, Tissier AM, Khairoune A, Khoury G, Eiss D, Hélénon O. Ultrasound elastography of the prostate: State of the art. Diagn Interv Imaging 2013;94:551–60.

Dark GG, Hill SA, Prise VE, Tozer GM, Pettit GR, Chaplin DJ. Combretastatin A-4, an agent that displays potent and selective toxicity toward tumor vasculature. Cancer Res 1997;57:1829–34.

Deffieux T, Gennisson J-L, Bousquet L, Corouge M, Cosconea S, Amroun D, Tripon S, Terris B, Mallet V, Sogni P, Tanter M, Pol S. Investigating liver stiffness and viscosity for fibrosis, steatosis and activity staging using shear wave elastography. J Hepatol 2015;62:317–24.

Doyley MM, Parker KJ. Elastography: general principles and clincial applications. Ultrasound Clin 2014;9:1–11.

El-Emir E, Boxer GM, Petrie I a, Boden RW, Dearling JLJ, Begent RHJ, Pedley RB. Tumour parameters affected by combretastatin A-4 phosphate therapy in a human colorectal xenograft model in nude mice. Eur J Cancer 2005;41:799–806.

Evans A, Whelehan P, Thomson K, McLean D, Brauer K, Purdie C, Baker L, Jordan L, Rauchhaus P, Thompson A. Invasive Breast cancer : Relationship between Shear-wave Prognostic Factors. Radiology 2012;263:673–7.

Evans A, Armstrong S, Whelehan P, Thomson K, Rauchhaus P, Purdie C, Jordan L, Jones L, Thompson A, Vinnicombe S. Can shear-wave elastography predict response to neoadjuvant chemotherapy in women with invasive breast cancer? Br J Cancer 2013;109:2798–802.

Fink SL, Cookson BT. Apoptosis, pyroptosis, and necrosis: mechanistic description of dead and dying eukaryotic cells. Infect Immun. 2005;73(4):1907-16.

Ganau S, Andreu FJ, Escribano F, Martin A, Tortajada L, Villajos M, Baré M, Teixidó M, Ribé J, Sentís M. Shear-wave elastography and immunohistochemical profiles in invasive breast cancer: Evaluation of maximum and mean elasticity values. Eur J Radiol 2014;84:617–22.

Gennisson J-L, Deffieux T, Fink M, Tanter M. Ultrasound elastography: Principles and techniques. Diagn Interv Imaging 2013;94:487–95.

Itoh A, Ueno E, Tohno E, Kamma H, Takahashi H, Shiina T, Yamakawa M, Matsumura T. Breast disease: clinical application of US elastography for diagnosis. Radiology 2006;239:341–50.

Juge L, Doan B-T, Seguin J, Albuquerque M, Larrat B, Mignet N, Chabot GG, Scherman D, Paradis V, Vilgrain V, Van Beers BE, Sinkus R. Colon Tumor Growth and Antivascular Treatment in Mice: Complementary Assessment with MR Elastography and Diffusion-weighted MR Imaging. Radiology 2012;264:436–44.

Kräling BM, Razon MJ, Boon LM, Zurakowski D, Seachord C, Darveau RP, Mulliken JB, Corless CL, Bischoff J. E-selectin is present in proliferating endothelial cells in human hemangiomas. Am J Pathol 1996;148:1181–91.

Lee JH, Kim SH, Kang BJ, Choi JJ, Jeong SH, Yim HW, Song BJ. Role and clinical usefulness of elastography in small breast masses. Acad Radiol 2011;18:74–80.

Nico B, Benagiano V, Mangieri D. Evaluation of microvascular density in tumors: pro and contra. Histol Histopathol 2008; 23: 601-607.

Nightingale K, McAleavey S, Trahey G. Shear-wave generation using acoustic radiation force: in vivo and ex vivo results. Ultrasound Med Biol 2003;29:1715–23.

Nguyen TM, Couade M, Bercoff J, Tanter M. Assessment of Viscous and Elastic Properties of Sub-Wavelength Layered Soft Tissues Using Shear Wave Spectroscopy: Theoretical Framework and In Vitro Experimental Validation. IEEE Trans Ultrason Ferroelectr Freq Control 2011;58(11):2305-2315.

Palmeri ML, Wang MH, Dahl JJ, Frinkley KD, Nightingale KR. Quantifying Hepatic Shear Modulus In Vivo Using Acoustic Radiation Force. Ultrasound Med Biol 2008;34:546–58.

Robl B, Botter SM, Pellegrini G, Neklyudova O, Fuchs B. Evaluation of intraarterial and intravenous cisplatin chemotherapy in the treatment of metastatic osteosarcoma using an orthotopic xenograft mouse model. J Exp Clin Canc Res 2016; 35:113.

Sarvazyan APA, Rudenko OO V, Swanson SD, Fowlkes JB, Emelianov SY. Shear wave elasticity imaging: a new ultrasonic technology of medical diagnostics. Ultrasound Med Biol 1998;24:1419–35.

Seguin J, Nicolazzi C, Mignet N, Scherman D, Chabot GG. Vascular density and endothelial cell expression of integrin alpha v beta 3 and E-selectin in murine tumours. Tumour Biol J Int Soc Oncodevelopmental Biol Med 2012;33:1709–17.

Seguin J, Doan B, Latorre Ossa H, Jugé L, Gennisson J, Tanter M, Scherman D, Chabot GG, Mignet N. Evaluation of Nonradiative Clinical Imaging Techniques for the Longitudinal Assessment of Tumour Growth in Murine CT26 Colon Carcinoma. Int J Mol Imaging 2013;2013:983534.

Tozer GM, Prise VE, Wilson J, Locke RJ, Vojnovic B, Stratford MR, Dennis MF, Chaplin DJ. Combretastatin A-4 phosphate as a tumor vascular-targeting agent: early effects in tumors and normal tissues. Cancer Res 1999;59:1626–34.

Viana CT, Campos PP, Carvalho LA, Cenedezi JM, Lavall L, Lopes MT, Ferreira MA, Andrade SP. Distinct types of tumors exhibit differential grade of inflammation and angiogenesis in mice. Microvasc Res 2013;86:44–51.

Wynn TA. Cellular and molecular mechanisms of fibrosis. J Pathol. 2008; 214(2):199-210.

Youk JH, Gweon HM, Son EJ, Kim JA, Jeong J. Shear-wave elastography of invasive breast cancer: Correlation between quantitative mean elasticity value and immunohistochemical profile. Breast Cancer Res Treat 2013;138:119–26.

Figure caption list

Figure 1: A) Shear modulus map in the central sagittal plane. Mean value within the ROI (5 mm diameter) is 5.1 ±2.3 kPa, maximum: 11.7 kPa and minimum: 1.0 kPa. B) Corresponding ultrasound image in the central sagittal plane.

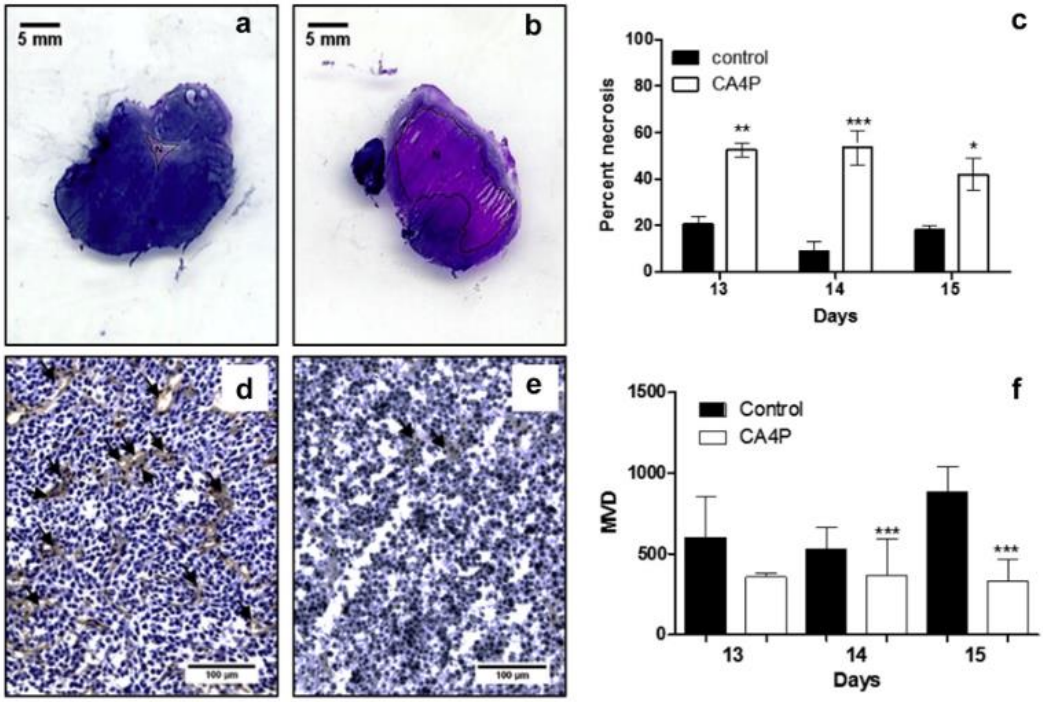

Figure 2: Longitudinal assessment of volume (A) and stiffness (B) from D5 to D12 post implantation of ectopic CT26 tumor obtained by ultrasound imaging and shear wave elastography. (Mean ± SEM n=52).

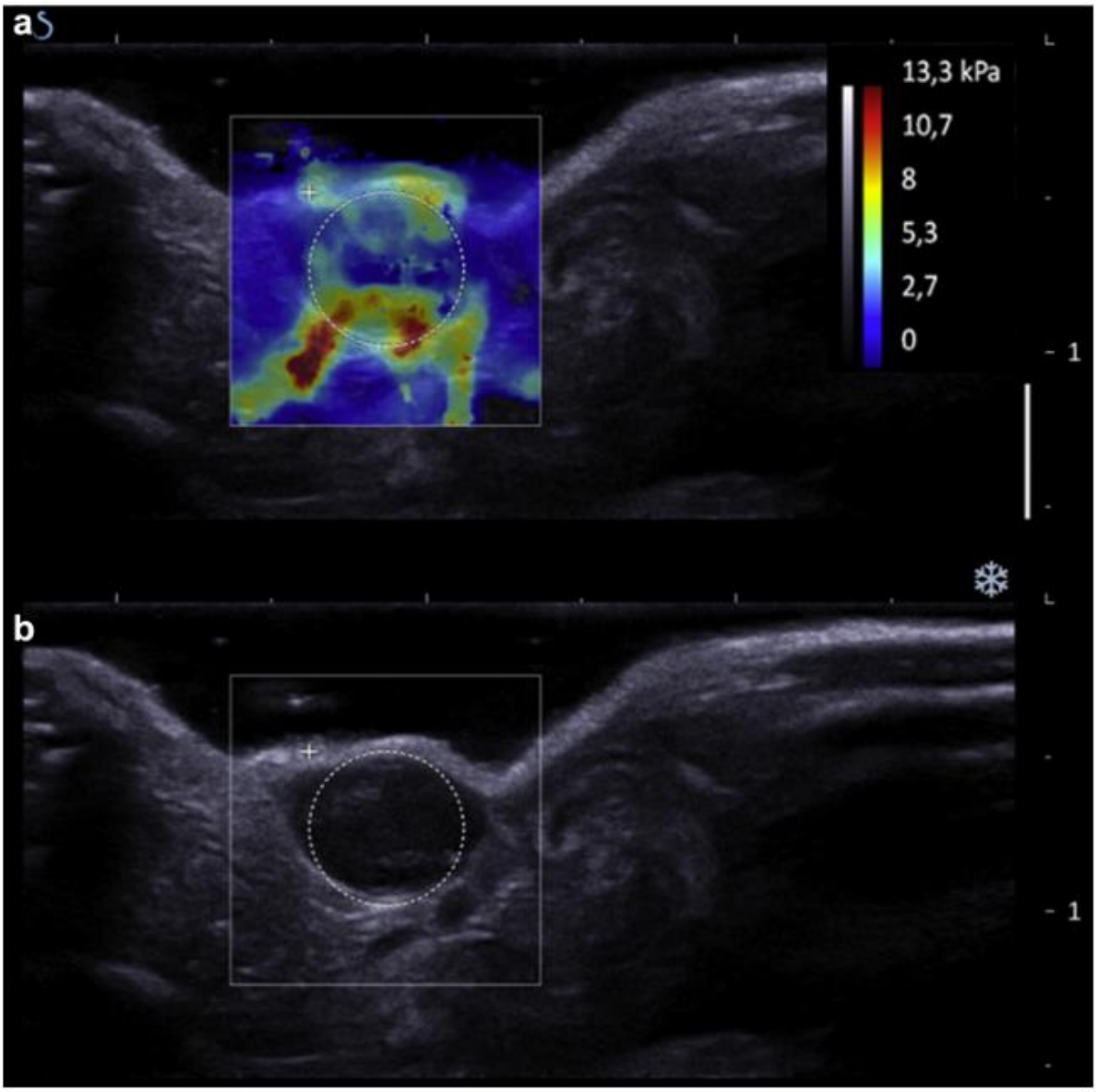

Figure 3: Longitudinal assessment of volume (A) and stiffness (B) of mice from D13 to D15 post implantation of ectopic CT26 tumor with and without CA4P treatment. Two-way ANOVA with Bonferroni posttests *** P<0.001. Values were obtained from Qbox measurements on the Aixplorer device.

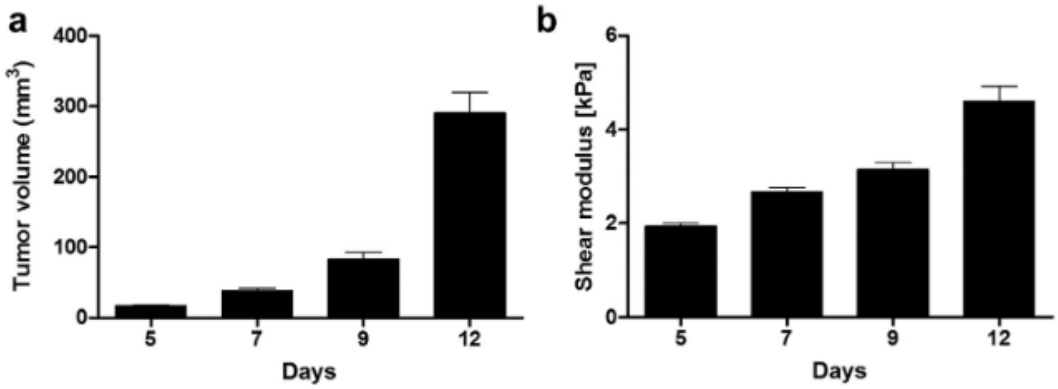

Figure 4: Histological images of the CT26 tumor at day 15 before (A) and after treatment (B) with CA4P and corresponding data of necrosis percent (C, n= 3, mean ±SEM). CD31 immunostaining of CT26 control (D) and treated (E) section 15 days after tumor implantation and corresponding data of MVD quantification (F, n= 3, mean ±SEM). Two-way ANOVA with Bonferroni posttests * P < 0.05, ** P<0.01, *** P<0.001.

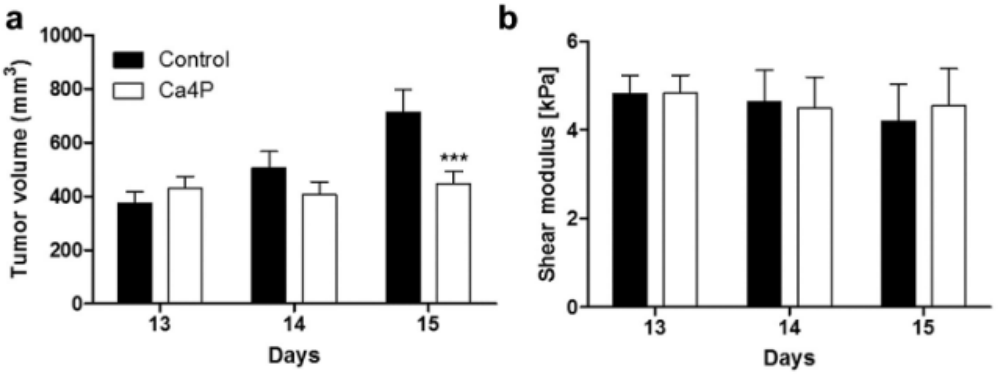

Figure 5: Procedure made for segmentation. Figure depicted in A tumor stiffness B the corresponding image in B-mode and in C the drawing area chosen for edges and center area (Blue). The corresponding data issue of the segmentation has presented as a function of time with or without CA4P treatment for the global tumor (D), the edges of the tumor (E) and the

center of the tumor (F).

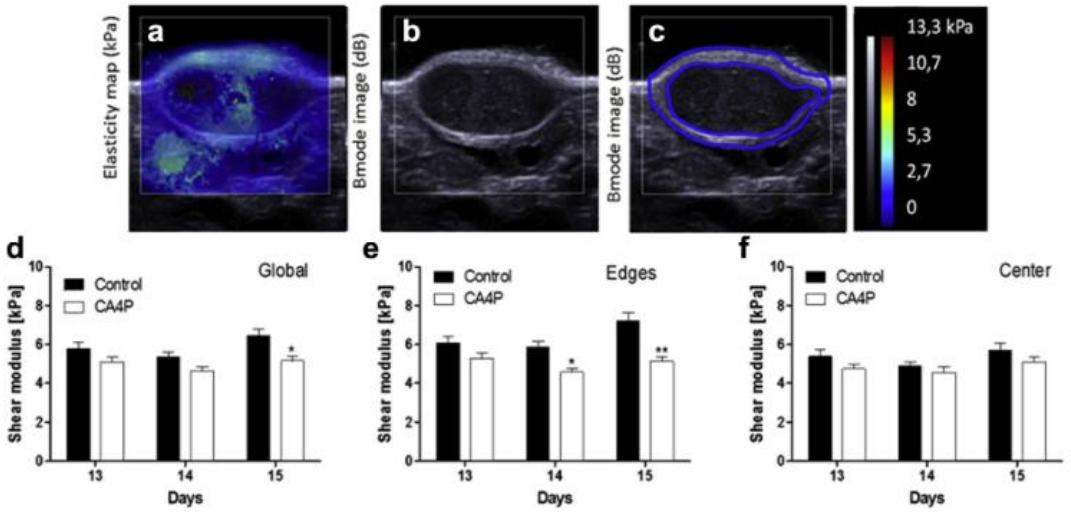

Table 1: Relative difference in stiffness (RD_{stiff}) normalized at day 12 (dimensionless) for each mice according to equation 1. Two-way ANOVA with Bonferroni posttests, *ns* not significant. Values were obtained from Qbox measurements on the Aixplorer device.

	Control		**CA4P**		**Two-way ANOVA**		
Days	**Mean ± SEM**	**n**	**Mean ± SEM**	**n**	**Difference**	**"P value"**	**Summary**
13	0.295 ± 0.071	26	0.041 ± 0.098	26	-0,254	"P > 0.05"	ns
14	0.198 ± 0.124	14	0.007 ± 0.126	22	-0,191	"P > 0.05"	ns
15	0.013 ±0.094	9	0.059 ± 0.140	19	0,045	"P > 0.05"	ns

Table 2: Necrosis area expressed in percentage hot spot (Mean ± SEM (n=3)) Two-way ANOVA with Bonferroni posttests, ns not significant, ** P < 0.01, *** P<0.001

	Center (%)		**Edges (%)**	
Days	Control	CA4P	Control	CA4P
13	50.69 ± 10.87	97.08 ±1.42, ***	34.63 ± 6.48	77.23 ± 18.43, ns
14	33.65 ± 1.47	98.97 ± 1.03, ***	9.86 ± 4.97	87.24 ± 12.34, **
15	54.53 ± 8.90	97.46 ± 2.54, ***	44.79 ± 13.94	80.23 ± 13.41, ns

Table 3: Fibrosis area expressed in percentage hot spot (Mean ± SEM (n=3)) Two-way ANOVA with Bonferroni posttests, ns not significant.

	Center (%)		**Edges (%)**	
Days	Control	CA4P	Control	CA4P
13	0.00 ± 0.00	0.00 ± 0.00 ns	0.69 ± 0.25	2.31 ± 0.75 ns
14	0.02 ± 0.02	0.59 ± 0.31 ns	1.96 ± 0.60	4.34 ± 2.08 ns
15	0.01 ± 0.01	0.69 ± 0.40 ns	2.27 ± 1.29	5.03 ± 0.98 ns